

Label-Free Raman Spectromicroscopy Unravels the Relationship between MGMT Methylation and Intracellular Lipid Accumulation in Glioblastoma

Nana Wang,[§] Jiejun Wang,[§] Pu Wang, Nan Ji,* and Shuhua Yue*Cite This: *Anal. Chem.* 2023, 95, 11567–11571

Read Online

ACCESS |



Metrics & More

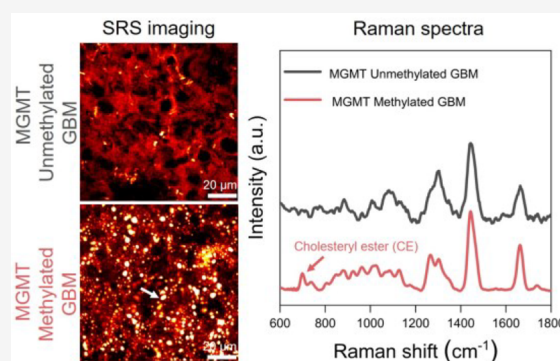


Article Recommendations



Supporting Information

ABSTRACT: Temozolomide (TMZ) is considered a first line chemotherapy drug for glioblastoma (GBM). Unfortunately, the GBM without methylation of O⁶-methylguanine-DNA methyltransferase (MGMT), accounting for about 70% of all GBM, shows an inherent resistance to TMZ treatment. Aberrant accumulation of neutral lipids, primarily triglycerides (TGs) and cholesteryl esters (CEs), in lipid droplets (LDs) has been recognized as metabolic vulnerability for GBM therapy. However, it is not known whether MGMT methylation affects lipid accumulation in GBM. Herein, we employed label-free Raman spectromicroscopy, which integrated stimulated Raman scattering (SRS) microscopy and confocal Raman spectroscopy, to quantitatively analyze both the amount and composition of intracellular LDs in intact GBM tissues obtained from patients who had undergone resection surgery. Our results showed significant reductions in both the LD amount and the CE percentage in MGMT unmethylated GBMs (MGMT methylation < 15%) compared to MGMT methylated ones (MGMT methylation ≥ 15%). Due to a big variation of lipid accumulation in the MGMT methylated GBMs, these patients were further divided into hypermethylated group (MGMT methylation ≥ 50%) and intermediate-methylated group (MGMT methylation 15~50%), according to the significantly different median survival rates of these two groups. Remarkable differences in LD amount, CE percentage, and also lipid saturation degree were found between the hypermethylated group and the other two groups, but not between the unmethylated and intermediate-methylated groups. To elucidate the possible underlying mechanism, we analyzed the differential expression of lipid metabolism-related genes in GBM with different levels of MGMT methylation using The Cancer Genome Atlas Program (TCGA) dataset. It was shown that the genes related to lipid oxidation and lipid efflux were upregulated, and the genes related to lipid synthesis were downregulated in unmethylated group. These findings unravel the relationship between MGMT methylation and lipid accumulation in GBM, which may offer new opportunities for the diagnosis and treatment of TMZ-resistant GBM.



INTRODUCTION

Glioblastoma (GBM) is the most common and malignant primary brain tumor with poor survival and high heterogeneity.¹ The current standard treatment for newly diagnosed GBM is surgical resection with concurrent radiation and alkylating chemotherapy, followed by adjuvant alkylating chemotherapy.^{2,3} Temozolomide (TMZ) treatment has been shown to increase the overall survival (OS) of GBM patients.^{4,5} The therapeutic benefits of TMZ depend on its ability to methylate DNA at the N⁷ and O⁶ positions of guanine and the N³ position of adenine.⁶ It has been found that GBM with methylation of the DNA repair enzyme O⁶-methylguanine-DNA methyltransferase (MGMT) is sensitive to TMZ, whereas GBM without MGMT methylation is resistant to TMZ.⁷ Currently, there is still no effective treatment available for MGMT unmethylated GBM, accounting for about 70% of all GBM.⁸

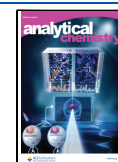
As a hallmark of human cancers, dysregulated lipid metabolism has been shown to induce intracellular accumulation of neutral lipids, primarily triglycerides (TGs) and cholesteryl esters (CEs), in lipid droplets (LDs).^{9–11} Aberrant neutral lipid accumulation has been recognized to be a vulnerable metabolic target for GBM treatment.^{12–14} Thus, it is intriguing to explore whether such lipid accumulation is universal for all GBM or related to MGMT methylation.

Due to limited spatial resolution or analytical capability, regular methods cannot provide information regarding LD distribution and composition at the same time as intact tissue,

Received: March 4, 2023

Accepted: July 3, 2023

Published: July 7, 2023



which hinders the study of LD biology in cancer. Owing to high chemical selectivity, submicron spatial resolution, and high imaging speed, stimulated Raman scattering (SRS) microscopy has shed new light on LD biology.^{15–17} Label-free Raman spectromicroscopy, which combines the fast chemical imaging capability of SRS microscopy and the full spectral analysis capability of spontaneous Raman spectroscopy on the same platform, permits quantitative analysis of not only the amount but also the composition of LDs in single cells.¹⁸ SRS spectral imaging has been applied to the study of lipid metabolism in various types of cancer, including prostate cancer,¹⁹ pancreatic cancer,²⁰ ovarian cancer,²¹ liver cancer,²² and melanoma.^{23,24} Particularly, SRS imaging revealed cisplatin-resistant cancer cell exhibited increased fatty acids (FA) uptake and oxidation.²⁵ Taken together, label-free Raman spectromicroscopy could provide new insights into the relationship between intracellular lipid accumulation and MGMT methylation in GBM.

Here, enabled by label-free Raman spectromicroscopy, we quantitatively analyzed lipid accumulation, including both the amount and composition of intracellular LDs in GBM tissues obtained from patients undergone resection surgery. Our results revealed significant reductions in both LD amount and CE percentage in MGMT unmethylated GBMs (MGMT methylation < 15%) compared to MGMT methylated ones (MGMT methylation \geq 15%). Considering the large heterogeneity of lipid accumulation within the MGMT methylated GBMs, we further divided MGMT methylated ones into hypermethylated group (MGMT methylation \geq 50%) and intermediate-methylated group (MGMT methylation 15~50%), based on the significant different median survival of these two groups. It was found that the hypermethylated group showed remarkable differences in lipid accumulation compared to the other two groups, whereas no significant difference was shown between the intermediate-methylated and unmethylated groups, suggesting the strong correlation between MGMT hypermethylation and lipid accumulation. Based on the TCGA dataset, we found a significant increase in lipid oxidation and lipid efflux and a decrease in lipid synthesis in the unmethylated group, which might result in the reduction of lipid accumulation. These findings collectively unravel the altered lipid metabolism in GBM with low MGMT methylation, which may open up new opportunities for the diagnosis and treatment of TMZ-resistant GBM.

RESULTS AND DISCUSSION

SRS Imaging and Raman Spectral Analysis of Intracellular Lipid Accumulation in MGMT Methylated and Unmethylated GBM. Based on label-free Raman spectromicroscopy, we performed a quantitative analysis of intracellular lipid accumulation in intact GBM tissues obtained from 36 patients undergone resection surgery. According to the current clinical practice, we grouped the GBMs into MGMT methylated GBMs (MGMT methylation \geq 15%, $n = 15$) and MGMT unmethylated GBMs (MGMT methylation < 15%, $n = 21$). By tuning the laser beating frequency to be resonant with C–H stretching vibration at 2850 cm^{-1} , strong SRS signals arose from the lipid-rich cell membranes and LDs, and in the meantime, weak signals were derived from the lipid-poor nuclei. Such an imaging contrast permits the clear visualization of cellular morphology and intracellular LDs in a label-free manner. As shown in Figure 1A,B, the SRS images

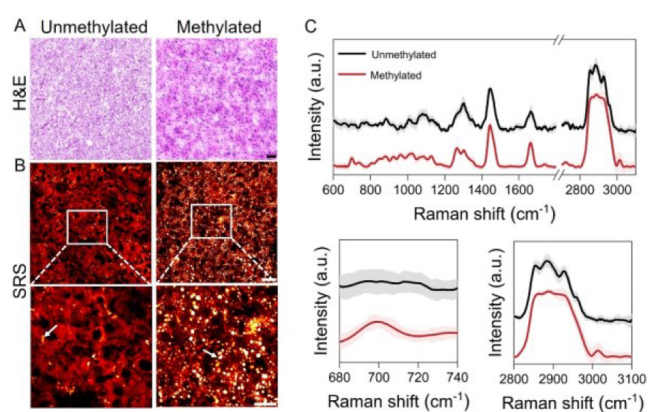


Figure 1. SRS imaging and Raman spectral analysis of lipid accumulation in methylated GBM (patient no. 35) and unmethylated GBM (patient no. 5). (A) H&E staining of the slices adjacent to the one for analysis by label-free Raman spectromicroscopy. Scale bar: 100 μm . (B) Representative SRS images of tissue slices from methylated GBM (patient no. 35) and unmethylated GBM (patient no. 5). Scale bar: 50 μm . Zoom-in images of the regions indicated by white boxes are shown in the bottom panel. LDs are indicated by white arrows. Scale bar: 20 μm . (C) Representative Raman spectra of LDs in GBM shown in (B). Spectral intensity was normalized by the CH_2 bending band at 1442 cm^{-1} . Shaded area indicates the standard deviation of Raman spectral measurements from different LDs in the same GBM tissue. In order to show the spectra more clearly, the spectra of unmethylated GBM (patient no. 5) were vertically shifted relative to methylated GBM (patient no. 35).

provided morphological information similar to the hematoxylin and eosin (H&E) images of the adjacent tissue slices. More importantly, we revealed a substantial reduction in intracellular lipid accumulation in MGMT unmethylated GBM (patient no. 5) compared to the methylated one (patient no. 35; Figure 1B). Further composition analysis of individual LDs by confocal Raman spectroscopy identified high CE level, based on the distinctive Raman peaks for cholesterol ring around 702 cm^{-1} and ester bond around 1742 cm^{-1} , in MGMT methylated GBM (patient no. 35) but not in MGMT unmethylated GBM (patient no. 5; Figure 1C). Meanwhile, since the distinctive Raman band peak at around 2883 cm^{-1} was found in saturated fat only (Figure S1), possibly originating from Fermi resonance or asymmetric vibration of CH_2 in a straight and long acyl chain,²² we characterized the lipid saturation level by the height ratio (I_{2883}/I_{2850}). As shown in Figure 1C, the lipid saturation level looked a little bit more prominent in MGMT unmethylated GBM (patient no. 5) than the methylated one (patient no. 35). Collectively, these findings unravel possible differences in lipid accumulation, including the LD amount and composition, between MGMT methylated and unmethylated GBMs.

Quantitative Analysis of the Correlation between Intracellular Lipid Accumulation and MGMT Methylation in GBM. The LD amount, quantified in the way of LD area fraction, for MGMT unmethylated GBMs, was only about one-third of that for the MGMT methylated GBMs (Figure 2A,B and Table S1), suggesting a significant reduction in the lipid accumulation in MGMT unmethylated GBMs. According to the quantitative method for CE percentage in the LD reported previously,^{19,26} we took the Raman spectra of mixed emulsions containing different molar ratios of TG and CE (Figure S2A) and found that the molar percentage of CE (CE percentage) out of the total neutral lipids was linearly

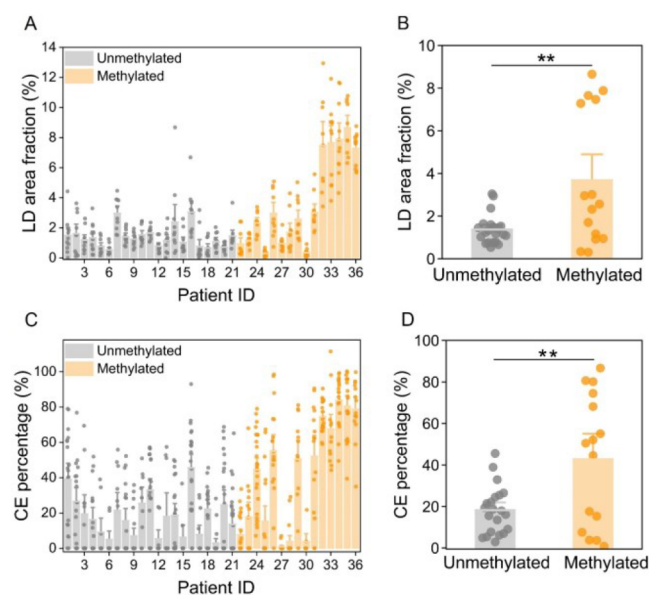


Figure 2. Quantitative analysis of the correlation between MGMT methylation and lipid accumulation in GBM. (A) LD area fraction derived from the SRS images in GBM tissues from 36 patients. (B) Average quantification of LD area fraction in (A) for unmethylated or methylated group. Each dot in (B) represents average LD area fraction for one patient. (C) Quantitation of CE percentage in GBM tissues from 36 patients. (D) Average quantification of CE percentage in (C) for unmethylated or methylated group. Each dot in (D) represents average CE percentage for one patient. Error bars represent SEM, $n > 10$. One-way ANOVA, $*p < 0.05$, $**p < 0.005$, $***p < 0.0005$.

proportional to the height ratio between the most prominent cholesterol band at 702 cm^{-1} and the CH_2 bending band at 1442 cm^{-1} (Figure S2B). According to this calibration curve, the CE percentage of LDs was significantly higher for MGMT methylated GBMs ($42.73\% \pm 8.20\%$) compared to that for MGMT unmethylated GBMs ($18.17\% \pm 2.51\%$; Figure 2C,D and Table S1). Considering that some LDs contained a high level of CEs while the others might not have detectable CEs, we also quantified the fraction of LDs with detectable CEs and the CE percentage within the LDs with detectable CEs, both of which significantly decreased in MGMT unmethylated GBMs relative to MGMT methylated ones (Figure S3). In addition, although some of the patients have a difference in lipid saturation level, no statistically significant difference was observed between MGMT methylated and unmethylated GBMs (Figure S4).

Notably, as shown in Figure 2B,D, there were clear clusters with high and low levels of LD amount or CE percentage in the MGMT methylated GBMs. For instance, some MGMT methylated GBMs did not show lipid accumulation as much as others did (Figure S5). This makes us speculate that the methylated population possibly has different subtypes. Based on The Cancer Genome Atlas (TCGA) dataset, we found a strong association between MGMT methylation and OS ($p < 0.005$, $df = 1$; Figure S6). Specifically, the GBMs with MGMT methylation $\geq 50\%$ evidently has a longer median survival (21.1 months) than the ones with a MGMT methylation of $15\sim 50\%$ (15.9 months) and the ones with a MGMT methylation $< 15\%$ (12.5 months; $p < 0.05$, $df = 1$; Figure 3A). Accordingly, MGMT methylated GBMs were further divided into hypermethylated-methylated (MGMT methylation $\geq 50\%$) and

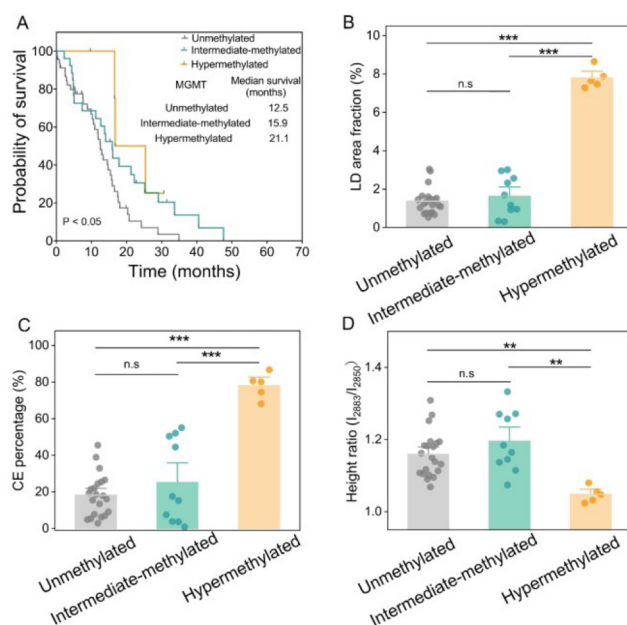


Figure 3. Quantitative analysis of lipid accumulation in GBM with different MGMT methylation. (A) OS of the patients in hypermethylated, intermediate-methylated, and unmethylated groups classified according to the median survival obtained from the TCGA dataset. Log-rank test $p < 0.05$, $df = 1$. LD area fraction (B), CE percentage (C), and height ratio (I_{2883}/I_{2850}) (D) in MGMT-hypermethylated, intermediate-methylated, and unmethylated groups. Each dot in (B) represents the average LD area fraction for one patient. Each dot in (C) represents the average CE percentage. Each dot in (D) represents the average height ratio (I_{2883}/I_{2850}) for one patient. Error bars represent SEM, $n > 10$. One-way ANOVA, $*p < 0.05$, $**p < 0.005$, $***p < 0.0005$.

intermediate-methylated (MGMT methylation $15\sim 50\%$) groups. As shown in Figure 3B, the LD amount was remarkably higher (>4.5 -fold) in the hypermethylated group compared to the other two groups. CE percentage was $78.01\% \pm 3.13\%$ in the hypermethylated group, which was also noticeably higher than that in the unmethylated group ($18.17\% \pm 2.51\%$) and intermediate-methylated group ($25.10\% \pm 7.15\%$; Figure 3C). The fraction of LDs with detectable CEs was also found to be distinctly increased (>2 -fold) in the hypermethylated group compared to the other two groups (Figure S7). In addition, the level of lipid saturation was significantly reduced in the hypermethylated group compared to the other two groups (Figure 3D), suggesting a higher lipid unsaturation level in hypermethylated GBMs. Interestingly, no significant differences in lipid accumulation were found between the unmethylated and intermediate-methylated groups.

Previous studies have reported that TGs and CEs are prevalent in GBM and could be used as potential targets.^{12–14,27} On one hand, we confirmed intracellular neutral lipid accumulation in GBM. On the other hand, we unveiled that such abundant lipid accumulation only occurred in the MGMT methylated GBM and especially the hypermethylated GBM, a newly recognized subtype benefiting from TMZ treatment the most. This suggests that the GBM with low MGMT methylation needs an alternative metabolic vulnerability for treatment.

Profiling of the Gene Expression Associated with the Reduction of Intracellular Lipid Accumulation in GBM without MGMT Methylation. Although some studies

showed the possible dysregulation of lipid metabolism in TMZ-resistance cell lines,^{28,29} the mechanism by which MGMT methylation affects lipid accumulation in GBM is unclear. Thus, we further explored the differential expression of lipid metabolism-related genes in hypermethylated, intermediate-methylated, and unmethylated groups, based on the TCGA dataset. The volcano plots displayed the differentially expressed genes (DEGs) in the three groups, and the common DEGs were then used for further functional analysis based on gene ontology (GO). ADTRP, which hydrolyzes bioactive fatty acid esters of hydroxy fatty acids,³⁰ was downregulated in the hypermethylated group relative to the unmethylated group (Figure 4A). CYP4F2 and CYP4F3, which eliminate excessive

effect from changes in the lipid synthesis, lipid uptake, lipid oxidation, and lipid efflux.

Furthermore, the GO analysis showed the downregulation of pathways related to lipid efflux, lipid transport, lipid catabolic process, and upregulation of pathways related to neutral lipid biosynthesis in hypermethylated groups relative to the other two groups (Figures 4D and S8–10). Together, these findings provide possible clues underlying the link between MGMT methylation and lipid accumulation in GBM.

CONCLUSIONS

In summary, enabled by label-free Raman spectromicroscopy, we surprisingly found out that the intracellular lipid accumulation, which was previously considered as a potent therapeutic target for GBM, occurred only in MGMT methylated GBM (TMZ-sensitive), particularly in the newly recognized hypermethylated GBM, but not in MGMT unmethylated GBM (TMZ-resistant). Thus, neutral lipid accumulation is not universal for all GBM and is probably related to MGMT methylation, which suggests that unmethylated GBM may need an alternative metabolic target for treatment. Moreover, we revealed that the increase of lipid efflux and lipid oxidation and the decrease of lipid synthesis potentially contributed to the reduced lipid accumulation in the GBM with low MGMT methylation. Our study unravels the hidden relationship between MGMT methylation and lipid accumulation in GBM, which may offer new markers for the detection of TMZ drug resistance and new targets for the treatment of MGMT unmethylated GBM.

ASSOCIATED CONTENT

Supporting Information

The Supporting Information is available free of charge at <https://pubs.acs.org/doi/10.1021/acs.analchem.3c00967>.

Information on the materials and methods, supplementary figures, and supplementary tables (PDF)

AUTHOR INFORMATION

Corresponding Authors

Shuhua Yue – Key Laboratory of Biomechanics and Mechanobiology (Beihang University), Ministry of Education, Institute of Medical Photonics, Beijing Advanced Innovation Center for Biomedical Engineering, School of Biological Science and Medical Engineering, Beihang University, Beijing 100191, China; orcid.org/0000-0003-1830-008X; Email: yue_shuhua@buaa.edu.cn

Nan Ji – Department of Neurosurgery, Beijing Tiantan Hospital, Capital Medical University, Beijing 100070, China; Email: jinan@mail.ccmu.edu.cn

Authors

Nana Wang – Key Laboratory of Biomechanics and Mechanobiology (Beihang University), Ministry of Education, Institute of Medical Photonics, Beijing Advanced Innovation Center for Biomedical Engineering, School of Biological Science and Medical Engineering, Beihang University, Beijing 100191, China

Jiejun Wang – Department of Neurosurgery, Beijing Tiantan Hospital, Capital Medical University, Beijing 100070, China

Pu Wang – Key Laboratory of Biomechanics and Mechanobiology (Beihang University), Ministry of Education, Institute of Medical Photonics, Beijing Advanced Innovation

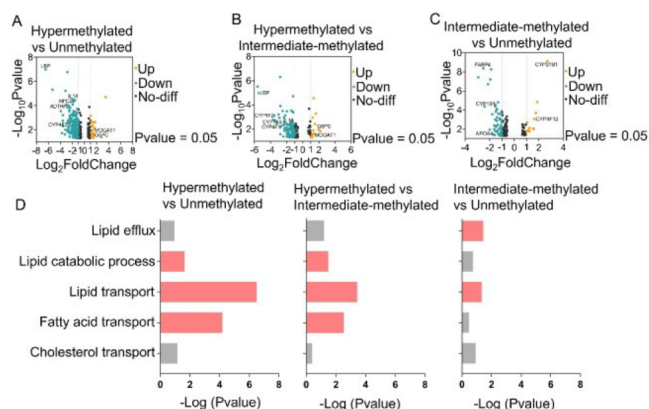


Figure 4. Analysis of lipid metabolism related gene expression in hypermethylated, intermediate-methylated, and unmethylated GBMs based on TCGA dataset. (A–C) Volcano plot of DEGs in hypermethylated vs unmethylated, hypermethylated vs intermediate-methylated, and intermediate-methylated vs unmethylated groups. DEGs were selected with thresholds of a fold change >2 and $p < 0.05$. (D) The common down-regulated pathways in hypermethylated vs unmethylated, hypermethylated vs intermediate-methylated, and intermediate-methylated vs unmethylated groups, obtained by GO enrichment analysis of DEGs. Red colors indicate a p value of less than 0.05, whereas gray colors indicate a p value greater than 0.05.

fatty acids,^{31,32} were downregulated in the hypermethylated group relative to intermediate-methylated and unmethylated groups (Figure 4A,B). IL18, whose deficiency was previously shown to induce lipid accumulation,³³ was downregulated in the hypermethylated group relative to the other two groups (Figure 4A,B). The de novo synthesis-related genes, such as MOGAT1 and G6PC, were upregulated in the hypermethylated group relative to the other two groups (Figure 4A,B). Collectively, these alterations of gene expression above led to the significant increase of lipid accumulation in the hypermethylated group compared to the other two groups.

In addition, to compare the intermediate-methylated group with the unmethylated group, we found the following changes in gene expression related to lipid metabolism (Figure 4C). The lipid synthesis related gene CYP1B1 and fatty acid uptake-related gene FABP4 were downregulated, whereas the fatty acid oxidation-related gene CYP4F12 was upregulated in intermediate-methylated group. Meanwhile, the cholesterol efflux-related gene APOA4 was downregulated in the intermediate-methylated group. These results together suggest that the big variation in the lipid accumulation in the intermediate-methylated group might be due to the synergistic

Center for Biomedical Engineering, School of Biological Science and Medical Engineering, Beihang University, Beijing 100191, China

Complete contact information is available at:

<https://pubs.acs.org/10.1021/acs.analchem.3c00967>

Author Contributions

[§]These authors contributed equally to this work.

Author Contributions

N.W. conducted the SRS image acquisition, Raman spectrum acquisition, and data analysis. J.W. conducted tissue preparation and participated in SRS imaging acquisition and Raman spectrum acquisition. P.W., S.Y., and N.J. were responsible for experimental design. N.W. wrote the manuscript. S.Y. and N.J. wrote and edited the manuscript. All authors contributed to the study and critically reviewed the manuscript.

Notes

The authors declare no competing financial interest.

ACKNOWLEDGMENTS

This work was supported by National Natural Science Foundation of China (No. 62027824), Fundamental Research Funds for the Central Universities (No. YWF-22-L-547), and The Capital Health Research and Development of Special (2022-2-2047).

REFERENCES

- (1) Uddin, M. S.; Mamun, A. A.; Alghamdi, B. S.; Tewari, D.; Jeandet, P.; Sarwar, M. S.; Ashraf, G. M. *Semin. Cancer Biol.* **2022**, *83*, 100–120.
- (2) Weller, M.; van den Bent, M.; Hopkins, K.; Tonn, J. C.; Stupp, R.; Falini, A.; Cohen-Jonathan-Moyal, E.; Frappaz, D.; Henriksson, R.; Balana, C.; Chinot, O.; Ram, Z.; Reifenberger, G.; Soffietti, R.; Wick, W. *Lancet. Oncol.* **2014**, *15* (9), e395–403.
- (3) Fisher, J. P.; Adamson, D. C. *Biomedicines* **2021**, *9* (3), 324.
- (4) Mirimanoff, R. O.; Gorlia, T.; Mason, W.; VandenBent, M. J.; Kortmann, R. D.; Fisher, B.; Reni, M.; Brandes, A. A.; Curschmann, J.; Villa, S.; Cairncross, G.; Allgeier, A.; Lacombe, D.; Stupp, R. *Journal of Clinical Oncology* **2006**, *24*, 2563–2569.
- (5) Tomar, M. S.; Kumar, A.; Srivastava, C.; Shrivastava, A. *Biochim. Biophys. Acta. Rev. Cancer* **2021**, *1876* (2), 188616.
- (6) Zhang, J.; Stevens, M. F. G.; Bradshaw, T. D. *Curr. Mol. Pharmacol.* **2012**, *5* (1), 102–114.
- (7) Wu, S.; Li, X.; Gao, F.; de Groot, J. F.; Koul, D.; Yung, W. K. A. *Neuro. Oncol.* **2021**, *23* (6), 920–931.
- (8) Wick, W.; Weller, M.; van den Bent, M.; Sanson, M.; Weiler, M.; von Deimling, A.; Plass, C.; Hegi, M.; Platten, M.; Reifenberger, G. *Nat. Rev. Neurol.* **2014**, *10* (7), 372–385.
- (9) Snaebjornsson, M. T.; Janaki-Raman, S.; Schulze, A. *Cell. Metab.* **2020**, *31* (1), 62–76.
- (10) Santos, C. R.; Schulze, A. *FEBS J.* **2012**, *279* (15), 2610–2623.
- (11) Cruz, A. L. S.; Barreto, E. A.; Fazolini, N. P. B.; Viola, J. P. B.; Bozza, P. T. *Cell. Death. Dis.* **2020**, *11* (2), 105.
- (12) Geng, F.; Cheng, X.; Wu, X.; Yoo, J. Y.; Cheng, C.; Guo, J. Y.; Mo, X.; Ru, P.; Hurwitz, B.; Kim, S. H.; Otero, J.; Puduvali, V.; Lefai, E.; Ma, J.; Nakano, I.; Horbinski, C.; Kaur, B.; Chakravarti, A.; Guo, D. *Clin. Cancer Res.* **2016**, *22* (21), 5337–5348.
- (13) Cheng, X.; Geng, F.; Pan, M.; Wu, X.; Zhong, Y.; Wang, C.; Tian, Z.; Cheng, C.; Zhang, R.; Puduvali, V.; Horbinski, C.; Mo, X.; Han, X.; Chakravarti, A.; Guo, D. *Cell Metab.* **2020**, *32* (2), 229–242.e8.
- (14) Guo, D.; Reinitz, F.; Youssef, M.; Hong, C.; Nathanson, D.; Akhavan, D.; Kuga, D.; Amzajerdi, A. N.; Soto, H.; Zhu, S.; Babic, I.; Tanaka, K.; Dang, J.; Iwanami, A.; Gini, B.; Dejesus, J.; Lisiero, D. D.; Huang, T. T.; Prins, R. M.; Wen, P. Y.; Robins, H. L.; Prados, M. D.; Deangelis, L. M.; Mellinghoff, I. K.; Mehta, M. P.; James, C. D.; Chakravarti, A.; Cloughesy, T. F.; Tontonoz, P.; Mischel, P. S. *Cancer Discovery* **2011**, *1* (5), 442–456.
- (15) Cheng, J. X.; Xie, X. S. *Science* **2015**, *350* (6264), aaa8870.
- (16) Yue, S.; Cheng, J. X. *Curr. Opin. Chem. Biol.* **2016**, *33*, 46–57.
- (17) Chen, T.; Yavuz, A.; Wang, M. C. *J. Cell. Sci.* **2022**, *135* (5), jcs252353.
- (18) Slipchenko, M. N.; Le, T. T.; Chen, H.; Cheng, J. X. *J. Phys. Chem. B* **2009**, *113* (21), 7681–7686.
- (19) Yue, S.; Li, J.; Lee, S. Y.; Lee, H. J.; Shao, T.; Song, B.; Cheng, L.; Masterson, T. A.; Liu, X.; Ratliff, T. L.; Cheng, J. X. *Cell. Metab.* **2014**, *19* (3), 393–406.
- (20) Li, J.; Gu, D.; Lee, S. S.; Song, B.; Bandyopadhyay, S.; Chen, S.; Konieczny, S. F.; Ratliff, T. L.; Liu, X.; Xie, J.; Cheng, J. X. *Oncogene* **2016**, *35* (50), 6378–6388.
- (21) Li, J.; Condello, S.; Thomes-Pepin, J.; Ma, X.; Xia, Y.; Hurley, T. D.; Matei, D.; Cheng, J. X. *Cell. Stem. Cell.* **2017**, *20* (3), 303–314.e5.
- (22) Yan, S.; Cui, S.; Ke, K.; Zhao, B.; Liu, X.; Yue, S.; Wang, P. *Anal. Chem.* **2018**, *90* (11), 6362–6366.
- (23) Du, J.; Su, Y.; Qian, C.; Yuan, D.; Miao, K.; Lee, D.; Ng, A. H. C.; Wijker, R. S.; Ribas, A.; Levine, R. D.; Heath, J. R.; Wei, L. *Nat. Commun.* **2020**, *11* (1), 4830.
- (24) Lee, H. J.; Chen, Z.; Collard, M.; Chen, F.; Chen, J. G.; Wu, M.; Alani, R. M.; Cheng, J. X. *BME. Front.* **2021**, *2021*, 9860123.
- (25) Tan, Y.; Li, J.; Zhao, G.; Huang, K. C.; Cardenas, H.; Wang, Y.; Matei, D.; Cheng, J. X. *Nat. Commun.* **2022**, *13* (1), 4554.
- (26) Wang, P.; Li, J.; Wang, P.; Hu, C. R.; Zhang, D.; Sturek, M.; Cheng, J. X. *Angew. Chem., Int. Ed.* **2013**, *52* (49), 13042–13046.
- (27) Wu, X.; Geng, F.; Cheng, X.; Guo, Q.; Zhong, Y.; Cloughesy, T. F.; Yong, W. H.; Chakravarti, A.; Guo, D. *iScience* **2020**, *23* (10), 101569.
- (28) Tiek, D. M.; Rone, J. D.; Graham, G. T.; Pannkuk, E. L.; Haddad, B. R.; Riggins, R. B. *Sci. Rep.* **2018**, *8* (1), 7222.
- (29) Nam, H. J.; Kim, Y. E.; Moon, B. S.; Kim, H. Y.; Jung, D.; Choi, S.; Jang, J. W.; Nam, D. H.; Cho, H. *iScience* **2021**, *24* (3), 102238.
- (30) Parsons, W. H.; Kolar, M. J.; Kamat, S. S.; Cognetta, A. B., III; Hulce, J. J.; Saez, E.; Kahn, B. B.; Saghatelian, A.; Cravatt, B. F. *Nat. Chem. Biol.* **2016**, *12* (5), 367–372.
- (31) Gasparrini, M.; Giampieri, F.; Alvarez Suarez, J. M.; Mazzoni, L.; Forbes Hernandez, T. Y.; Quiles, J. L.; Bullon, P.; Battino, M. *Curr. Drug Targets* **2016**, *17* (8), 865–889.
- (32) Wanders, R. J.; Komen, J.; Kemp, S. *FEBS J.* **2011**, *278* (2), 182–194.
- (33) Netea, M. G.; Joosten, L. A.; Lewis, E.; Jensen, D. R.; Voshol, P. J.; Kullberg, B. J.; Tack, C. J.; van Krieken, H.; Kim, S. H.; Stalenhoeef, A. F.; van de Loo, F. A.; Verschuere, I.; Pulawa, L.; Akira, S.; Eckel, R. H.; Dinarello, C. A.; van den Berg, W.; van der Meer, J. W. *Nat. Med.* **2006**, *12* (6), 650–656.